JOURNAL OF BIOMEDICAL OPTICS 2(3), 295–303 (JULY 1997)

TEMPERATURE DISTRIBUTION IN *ESCHERICHIA COLI* LIQUID SUSPENSIONS DURING IRRADIATION BY A HIGH-POWER ND:YAG LASER FOR STERILIZATION APPLICATIONS

Ruikang K. Wang,[†] Ian A. Watson,[†] Glenn D. Ward,[†‡] Duncan E. S. Stewart-Tull,[‡] and Alastair C. Wardlaw[‡]

[†]Glasgow University, Laser and Optical Systems Engineering Center, Department of Mechanical Engineering, Glasgow G12 8QQ, United Kingdom; [‡]University of Glasgow, Division of Infection and Immunity, Joseph Black Building, Glasgow G12 8QQ, United Kingdom

(Paper JBO-125 received Dec. 5, 1996; revised manuscript received May 14, 1997; accepted for publication May 21, 1997.)

ABSTRACT

A time-dependent, heat diffusion equation was used to predict the three-dimensional temperature distribution of *Escherichia coli* in liquid-suspension during irradiation by a high-power Nd:YAG laser. The model may be used to calculate the temperature rise and the transient 3-D temperature profile in the liquid suspension under arbitrary combinations of laser wavelength, pulse shape, pulse width, repetition rate, energy density, and for different concentrations of bacteria. The temperature profiles in the liquid, for a range of energy densities, were measured to validate the theoretical model. The experimental results were in good agreement with the theoretical ones. A temperature gradient was found in the sample in the radial and axial directions during laser irradiation. The model enables the parameters that affect the temperature distribution of the liquid suspension to be identified and optimized when designing laser sterilization systems. © *1997 Society of Photo-Optical Instrumentation Engineers.* [S1083-3668(97)00803-4]

Keywords liquid suspension; Nd:YAG laser; sterilization; diffusion equation.

1 INTRODUCTION

Saks and Roth[1] demonstrated in 1963 that ruby lasers had significant biocidal capacity against *Spirogyra* and amoebas. Since then, interest has been focused on dental[2] and medical[3] sterilization or inactivation applications, many of which use photosensitizers[4] and low-power lasers. Recently, investigations into the biocidal capacity of various lasers to inactivate *Escherichia coli*[5] lawned on agar plates showed that high-power Nd:YAG and CO_2 lasers were effective. Moreover, the specificity of Nd:YAG laser radiation to a range of bacteria has been quantified.[6] However, earlier works investigating laser sterilization were all based on experimental comparisons; the quantitative modeling of the mechanism of biocidal activity of lasers is timely. Many possible mechanisms have been suggested,[7] such as photothermal, photochemical, and photoablation mechanisms. The sterilization mechanism will be dependent on the laser wavelength. For lasers operating in the infrared, one common observation is that a large amount of heat is generated during irradiation; this will heat up the bacteria, leading to a killing mechanism that is at least partly thermal. However, it is still not known whether other processes are occurring that may contribute to the killing effect.

One of the problems in identifying and isolating other factors is that the death rate due to thermal effects for laser irradiation is not known precisely. This is because of the large temperature gradients that exist within the sample being irradiated and the difficulty of measuring these accurately and obtaining a suitable control that can replicate the heating effect of the laser to allow a comparison between laser and thermal effects. Consequently, because the biocidal effect caused by laser irradiation may be related to heat generation, it is reasonable to believe that such an effect can be, partly at least, predicted from knowledge of the temperature in the target containing the bacteria. Methods for theoretically calculating the whole temperature field based on heat transfer principles have there-

Current affiliation of Ruikang Wang: Keele University, Dept. of Biomedical Engineering and Medical Physics, North Staffordshire Hospital, Hartshill, Stoke-on-Trent ST4 7QB, United Kingdom. Address all correspondence to Ruikang Wang. E-mail: bea03@cc.keele.ac.uk

fore been developed to find the temperature gradients induced in samples, and predict the effect of laser irradiation on bacteria. This will allow the thermal effect to be quantified accurately and will help to indicate whether processes other than thermal ones are occurring.

Computer simulation methods to evaluate the target temperature rise induced by laser exposure have been extensively carried out in medicine and surgery by several investigators.[8–10] The models generally involve a two-dimensional partial differential equation, and the laser energy function is introduced by appropriate choice of boundary conditions. Often, the wavelength- and temperature-dependent absorption coefficient of the sample and the temperature-dependent thermal coefficients of the material, such as the thermal conductivity and diffusivity, are neglected. The model developed here is similar, in essence, to some previous models, but it is more flexible and accurate in that it considers the temperature dependence of these parameters for a specific wavelength.

The purpose of the present work is to develop a mathematical model that can be used to estimate the whole temperature field of a laser-irradiated target associated with the system parameters, for example, wavelength, pulse shape, energy density, and bacteria concentration. Moreover, all the parameters that directly affect the temperature can be identified. Such information may be very helpful in establishing laser operating parameters that optimize the effectiveness of the laser's killing capacity.

2 THE MODEL

The mathematical model developed here was designed to calculate the temperature distribution within the target, incorporating various irradiation conditions, such as spatial distribution of energy and temporal behavior of the laser beam. Moreover, the model had to be readily adaptable to various conditions and to specific applications.

A rational and general starting point for analysis of the temperature distribution in a system is the standard three-dimensional transient diffusion equation:

$$\frac{\partial T}{\partial t} = \nabla \alpha(T) \nabla T + \frac{Q}{\rho c}, \tag{1}$$

where T is the temperature change (°C) from ambient conditions; t is the time in seconds (s); α denotes thermal diffusivity (cm^2/s); ρ is mass density (g/cm^3); c is the heat capacity (J/g/°C); and Q is the internal heat generated by the laser source (W/cm^3). The temperature T is defined as the temperature difference between the actual target temperature T_1 and the ambient temperature T_0, rather than the absolute value.

Laser beams usually have a cylindrical symmetry; this feature leads to reducing a 3-D problem to a 2-D problem, and use of the axisymmetrically cylindrical coordinate system in the mathematical model. Figure 1 shows the geometry of a bacterial liquid suspension contained in a vessel and irradiated by a laser beam. The vessel is L deep with diameter R. Therefore, in cylindrical coordinates, Eq. (1) can be represented by the following two-dimensional equation:

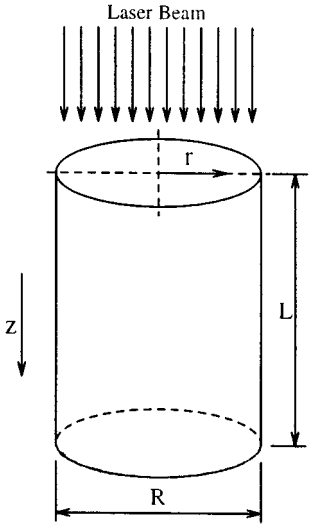

Fig. 1 Schematic of laser irradiation to sample.

$$\frac{\partial T}{\partial t} = \frac{\partial}{\partial z}\left(\alpha \frac{\partial T}{\partial z}\right) + \frac{\alpha}{r}\frac{\partial T}{\partial r} + \frac{\partial}{\partial r}\left(\alpha \frac{\partial T}{\partial r}\right) + \frac{Q(z,r,t)}{\rho c}. \tag{2}$$

The initial whole temperature field within the target was assumed to be uniform and equal to the temperature of the ambient air. This assumption leads to the following initial condition:

$$T = 0 \quad \text{at} \quad t = 0. \tag{3}$$

At all boundaries of the target, heat loss occurs as a result of convection and radiation. However, only convection is significant[11]; this results in the following boundary conditions:

$$\frac{\partial T}{\partial z} = \frac{h_1}{k} T, \quad \text{at } z = 0 \tag{4a}$$

$$\frac{\partial T}{\partial z} = -\frac{h_2}{k} T, \quad \text{at } z = L \tag{4b}$$

$$\frac{\partial T}{\partial r} = -\frac{h_3}{k} T, \quad \text{at } r = R, \tag{4c}$$

where h_1, h_2, and h_3 are the convection coefficients, ($J/s/cm^2$), at the top surface, bottom surface, and side wall of the target body, respectively; and k is the thermal conductivity (J/s/cm/°C) of the sample. Natural convection from the sides of

the sample was assumed and the following equation, taken from Holman,[11] was applied:

$$h = h_1 = h_2 = h_3 = 1.43 \times 10^{-4} (T)^{1/3} \quad (\mathrm{W/cm^2}). \tag{5}$$

This is a reasonable assumption since the temperature of the liquid suspension is normally under 100 °C[11] due to the limited laser exposure needed to cause sterility and/or inactivation.

The internal heat generation, $Q(z,r,t)$, may take on various forms, depending on the system and process of interest. For example, in living tissues there may be convective heat exchange between blood perfused through the local microvascular network and the surrounding tissue under conditions in which the blood and tissue are at different temperatures.[12] However, here, the target samples are treated with lasers. Thus, an internally distributed energy source is created owing to the absorption properties of the samples when they are irradiated with laser light. Assuming that the deposition of energy in the sample due to laser irradiation follows a Lambert–Beer absorption distribution, the energy source $Q(z,r,t)$ due to the absorption of light is given by

$$Q(z,r,t) = S(r) E(\lambda,t) \beta(\lambda,T) \exp[-\beta(\lambda,T) z], \tag{6}$$

where $S(r)$ is a dimensionless representation of the laser beam spatial energy distribution function; $E(\lambda,t)$, $(\mathrm{W/cm^2})$, is the peak energy density at wavelength λ and time t; $\beta(\lambda,T_1)$ is the absorption coefficient of the sample at the wavelength λ (cm) and temperature T_1, where $T_1 = T + T_0$. If the laser beam spatial distribution takes on a Gaussian-shaped profile, $S(r)$ in Eq. (6) is given by

$$S(r) = \exp\left(\frac{-2r^2}{a^2}\right), \tag{7a}$$

where a is the radius of the beam at the point where the beam intensity has reduced to $1/e^2$ of the peak value, whereas for a laser beam with a top-hat mode shape, $S(r)$ is given by

$$S(r) = \begin{cases} 1, & \text{when } r \leq r_0 \\ 0, & r > r_0 \end{cases}, \tag{7b}$$

where r_0 is the laser beam radius.

Equation (6) is adequate for the case of CW laser beams. However, pulsed lasers are frequently used in many applications. In this case, the laser heat source is time dependent and can be expressed as

$$E(\lambda,t) = E(\lambda) P(t), \tag{8a}$$

where

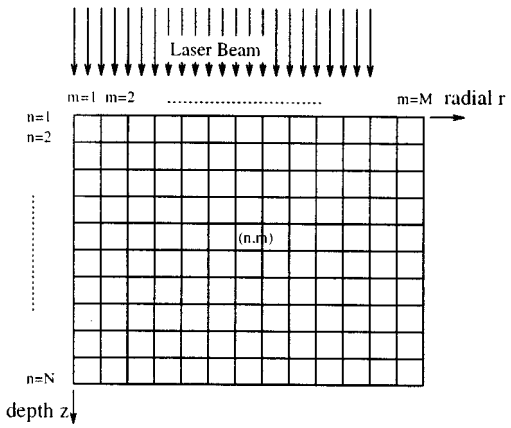

Fig. 2 Grid arrangement for finite-difference method.

$$P(t) = \begin{cases} 1, & \text{when the laser pulse is ''on''} \\ 0, & \text{when the laser pulse is ''off''.} \end{cases} \tag{8b}$$

However, the functions $S(r)$ and $P(t)$ can be assigned according to actual experimental measurements to improve the model's accuracy.

From Eq. (2) to Eq. (8), it can be seen that this model has the following advantages: (1) The laser energy is introduced as a heat source term in the differential equation and not via the boundary conditions. This allows wavelength- and temperature-dependent absorption of laser energy to be considered. (2) The model incorporates the spatial energy distribution and temporal behavior of the laser beam; this allows the temperature profile to be calculated under various laser irradiation conditions. (3) The temperature-dependent thermal diffusivity is considered in the model, making the predicted temperature profiles more accurate.

3 SOLVING THE THERMAL DIFFUSION EQUATION

To solve the thermal diffusion equation [Eq. (2)], many analytical methods could be used, and some methods allow computation of the exact steady-state temperature. These solutions are not convenient because they do not give the transient temperature profiles and they are prohibitive in terms of computational time to find the analytical solution. The numerical solution, however, is an approximation of the exact solution and allows computation of transient temperature profiles in a relatively short period of time. The finite-difference method is one of the main tools used to solve this kind of differential equation, and it was adapted here to solve the thermal diffusion equation (2). This equation was formulated into a set of finite-difference equations that could be solved for a grid appropriate to the problem of interest. Figure 2 shows the finite-difference arrangement of the grid. The subscripts n and m are used to specify the

nodes at grid intersections, representing the axial and radial increments respectively, and the subscript k is used to specify the time step.

A Peaceman–Rachford procedure,[13] i.e., the alternative-direction implicit (ADI) method, was used for the finite-difference method as follows:

$$\left.\frac{\partial T}{\partial t}\right|_{n,m,k+1/2} = \frac{2}{\Delta t_k}\left[T_{n,m,k+1/2} - T_{n,m,k}\right] \quad (9a)$$

$$\Delta t_k = t_{k+1} - t_k \quad (9b)$$

$$\left.\frac{\alpha}{r}\frac{\partial T}{\partial r}\right|_{n,m,k} = \frac{\alpha_{n,m}}{2m(\Delta r)^2}\left[T_{n,m+1,k} - T_{n,m-1,k}\right] \quad (9c)$$

$$\left.\frac{\partial}{\partial r}\left(\alpha\,\frac{\partial T}{\partial r}\right)\right|_{n,m,k} = \frac{\alpha_{n,m}}{(\Delta r)^2}\left[T_{n,m+1,k} - 2T_{n,m,k} + T_{n,m+1,k}\right] \quad (9d)$$

$$\left.\frac{\partial}{\partial z}\left(\alpha\,\frac{\partial T}{\partial z}\right)\right|_{n,m,k} = \frac{\alpha_{n,m}}{(\Delta z)^2}\left[T_{n,m+1,k} - 2T_{n,m,k} + T_{n,m+1,k}\right], \quad (9e)$$

where $\alpha_{n,m}$ is the thermal diffusivity corresponding to the local temperature at that location. In the ADI method, every time step is divided into two half-time steps. During the first half-time step, the axial gradients are treated explicitly while the radial gradients are treated implicitly, whereas in the second half-time step, the axial gradients are treated implicitly while the radial gradients are treated explicitly. This is done simultaneously over the 2-D mesh for each time step.

Using the ADI algorithm, Eq. (2) can be solved with the boundary conditions controlled by Eqs. (3) through (4). Note that the ADI algorithm can be easily adapted to be used with a variable-sized grid; this may be used when the absorption of the sample is high, such as for laser sterilization of surfaces.

The model and algorithm were implemented on a SunSpark workstation. A software package was specially developed in C^{++} language that allowed calculations of the 3D transient temperature distributions in the target. The graphical representations were made using the Matlab software package. The mean computation time was less than 50 ms per time step to calculate and store the temperature distribution in the target sample.

4 THEORETICAL AND EXPERIMENTAL RESULTS

4.1 MATERIAL AND EXPERIMENTAL DESCRIPTION

A liquid suspension (phosphate-buffered saline, PBS) of *Escherichia coli* B10537 was used in the experiments to verify the mathematical model developed; the *E. coli* suspension was obtained from the culture collection at the University of Glasgow, where it is maintained on nutrient agar (Oxoid) slope at 4 °C and subcultured once monthly. The bacterial suspension was pipetted into a sterile vessel and irradiated with a 1.06-μm Nd:YAG laser beam; the initial temperature was 22.6 °C. The concentration of the *E. coli* in PBS was 10^6 cells/ml and, based on the previous experiments, assumed to have the same thermal and optical properties as water. Table 1 gives data for the temperature-dependent parameters[14] that were used in the model. These data were input into the mathematical model using a look-up table so that the theoretical temperature profile of the sample could be calculated. A linear interpolation was used to find the values of parameters for temperatures in-between those stated in Table 1.

Table 1 Temperature dependence of heat capacity, thermal conductivity, and thermal diffusivity of water.

Temperature (°C)	Heat capacity (J g^{-1} K^{-1})	Thermal conductivity $\times 10^{-5}$ (W cm^{-1} K^{-1})	Thermal diffusivity $\times 10^{-5}$ (cm^2 s^{-1})
20	4.183	603	144.2
25	4.181	611	146.1
30	4.179	618	147.9
35	4.178	625	149.6
40	4.179	632	151.2
45	4.181	638	152.6
50	4.182	643	153.8
55	4.183	648	154.9
60	4.185	653	156.0
65	4.188	658	157.1
70	4.191	662	158.0
75	4.194	666	158.8
80	4.198	670	159.6
85	4.203	673	160.1
90	4.208	676	160.6
95	4.213	678	160.9
100	4.219	681	161.4

The absorption coefficient for the *E. coli* liquid suspension (10^6 ml^{-1}) at the Nd:YAG laser wavelength $\lambda = 1.06\,\mu$m was determined from Beer's law. An absorption coefficient value of 0.10 cm^{-1} was used throughout these simulations.[15] The the-

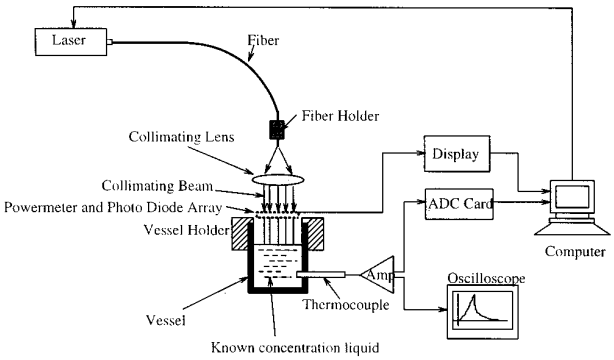

Fig. 3 Experimental setup.

oretical results obtained using this value were consistent with those obtained from the experiments.

The laser (Lumonic's MS830; Ruby, UK) was operated at 10 J of pulsed energy, a 10-Hz pulse repetition rate, and an 8-ms pulse width. A beam diameter of 1.1 cm was used. The laser power was measured at the target site using a Laser Precision RT 3000 power meter. A small fraction of the beam was sampled using a wedge. A linear photodiode array was used to measure the spatial profile and diameter of the laser beam. The pulse width was measured using an oscilloscope. The beam mode was assumed to be the top-hat-shaped profile.

The experimental system is shown in Figure 3. A fiber optic beam delivery system was used with a collimating and focusing lens assembly. A glass vessel was placed underneath the collimated beam in a holder, which ensured accurate repositioning of the vessel relative to the incident beam. The vessel was 3.0 cm high and had an inner diameter of 1.3 cm. A thermocouple with a response speed of 0.1 s was placed into the vessel 2.11 cm from the top surface; it was near the side wall but shielded from the laser beam to prevent the beam from directly heating it. The thermocouple was calibrated using a standard water bath and mercury thermometer, and was used to measure the transient temperature rise of the liquid during irradiation by the laser beam. The output voltage from the thermocouple was amplified, signal conditioned, and fed into an analog-to-digital converter card in a PC-486 computer. The laser output power was controlled so that when the measured temperature reached 50 °C, which took approximately 21.6 s from the initial ambient temperature of 22.6 °C, the laser was turned off.

4.2 RESULTS

By solving the heat diffusion equation, the transient temperature profiles of the liquid culture were found. The theoretical temperature at the positions where the thermocouple was placed in the vessel was compared with the measured temperature. The laser was turned off after 21.6 s, both experimentally and in the model. The temperature was still calculated and measured so that the cooling curve could be modeled and compared with the experimental results; this allowed the complete temperature-time history of the bacterial suspension to be ascertained.

Figures 4(a) through 4(d) illustrate the transient temperature profiles on the cross-section plane that goes through the central axis at 1, 10, 21.6, and 35 s, respectively. It is seen that the temperature rises most rapidly at the center of the vessel and just below the surface of the liquid, reaching a peak value of 90.5 °C at a depth 0.3 cm below the surface, just after 21.6 s. By 35 s, this temperature had decreased to 80.3 °C. The temperature rise decreases as the distance is increased from the center of the vessel. Figures 5(a) through 5(d) give the temperature profiles on the plane that is perpendicular to the central axis and 0.3 cm away from the top surface, respectively, for the same times as quoted for Figure 4. Owing to the absorption of the laser energy and conduction of heat, the temperature at any point increases with the exposure time. Initially, the temperature rise in the sample is dominated by the absorption of the laser energy. As can be seen from Figure 4(a) and Figure 5(a), the temperature profile inside the exposed region is quite flat but higher than the initial ambient temperature, whereas in the regions that are not irradiated by the laser beam, the temperature stays almost at the initial temperature. A sudden temperature rise on the edge of the laser beam can be seen clearly. With increasing exposure, the temperature inside the laser beam area continues rising due to absorption of the laser energy and at the same time, the temperature outside the exposed region starts to increase due to lateral diffusion of heat. At the time the laser was turned off, i.e., at 21.6 s, the surface temperature inside the exposed region had reached its maximum value, while the temperature continued increasing outside the beam region due to conduction (see Figure 8 for more details). Figures 4 and 5 show that a temperature gradient exists in both the radial and the axial directions. If laser sterilization is at least partly thermally dependent, then such temperature gradients indicate that bacteria are more likely to survive laser exposure in the region near the side of the vessel and near its bottom. However, in the present case no account has been taken of eddy currents or turbulence.

As previously mentioned, the maximum temperature reached in the target sample occurs several millimeters below the surface. This is due to the heat losses from the surface, leading to a surface temperature slightly lower than that at the place just beneath the surface, where convective losses do not occur.

Figure 6(a) shows the temperature rise as a function of depth for different radial distances from the center of the exposed region. Figure 6(b) shows the temperature profiles as a function of radial distance from the center of the beam for different depths. It

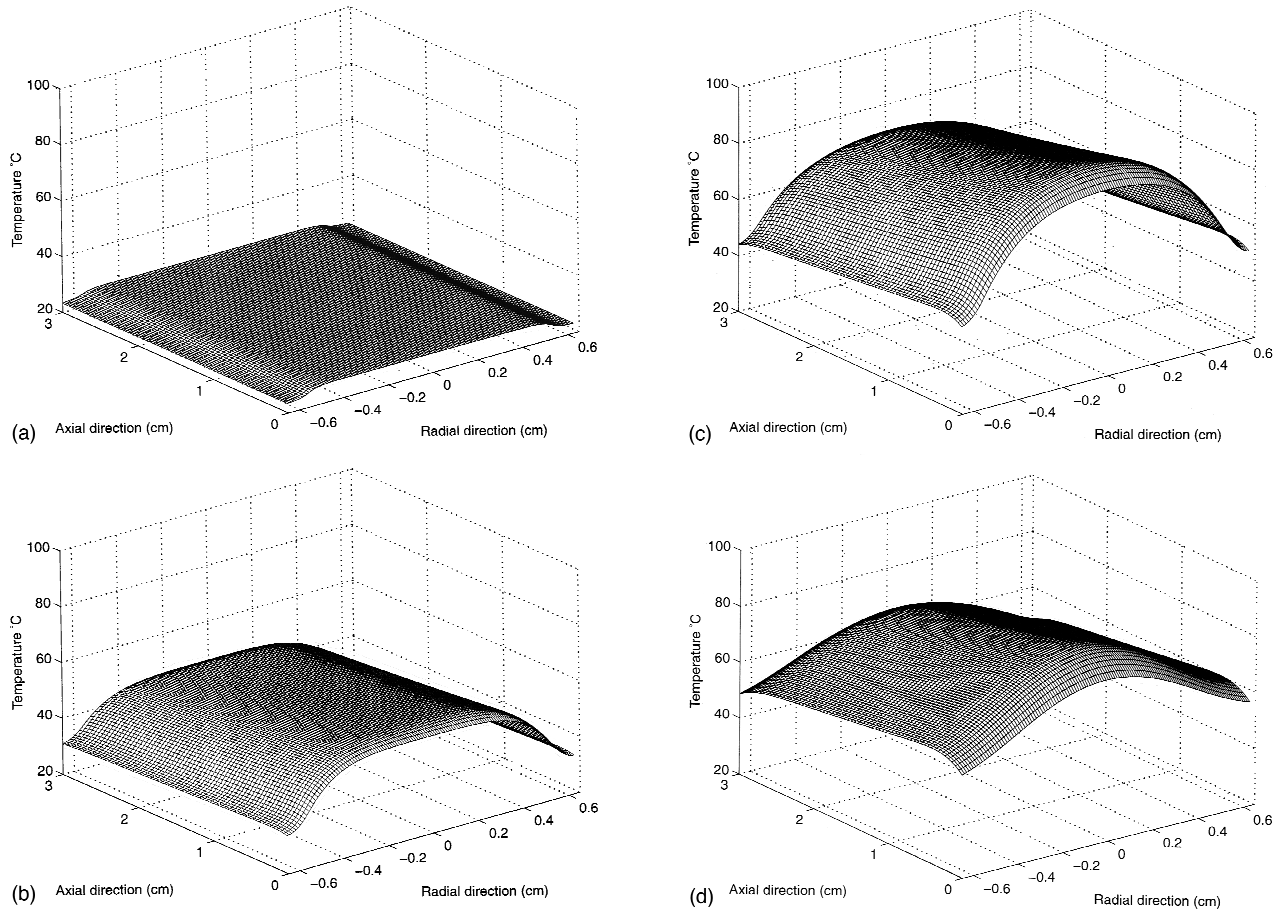

Fig. 4 The transient temperature profiles on the cross-section plane that goes through the central axis at the instant of: (a) 1 s, (b) 10 s, (c) 21.6 s, and (d) 35 s, respectively.

can be seen that the maximum temperature difference from the center to the side wall is about 45 °C, and the temperature gradient in the radial direction is greatest for $z = 0.3$ cm. Even inside the central half-beam region, an approximately 25 °C temperature difference was obtained. The maximum temperature rise is 90.5 °C, which means that the bacteria around this region are unlikely to survive, whereas the minimum temperature rise is 43.1 °C, which may be below the lethal temperature threshold to kill bacteria.[16] Thus, the bacteria in regions where the temperature is higher than the lethal temperature threshold would be killed, whereas those outside that region would probably survive.

Figure 7(a) illustrates a gray-level image representation of the temperature profile of Figure 4(c) at the instant the laser was turned off, where the black level represents a temperature value of 40 °C and the white level represents a temperature of 100 °C. The temperature gradient can be seen from this gray image illustration. The dark regions have a lower temperature, and bacteria in this area are less likely to be killed or inactivated, whereas in the bright region, cell death is highly likely for this exposure time. Figure 7(b) shows a contour plot of the isothermal zones in the liquid suspension. From either Figure 7(a) or 7(b), the sterilized zone in the liquid suspension can be identified if the lethal temperature threshold is known *a priori*. Moreover, gray-level images for energy density could be produced to indicate likely areas where sterilization or inactivation will occur. In an attempt to show the sterilization boundaries, 65 °C was taken to be the lethal threshold temperature for the *E. coli* under the laser treatment. Thus, Figure 7(c) illustrates the sterilization zones in the liquid suspension for the present case, where the gray area represents the sterilized zone and the black region is the area where bacteria could survive. By changing the model to accommodate, for example, the different beam sizes and sample sizes and depths, optimum designs for a laser sterilization system can be built to maximize the volume of liquid sterilized. This demonstrates the importance of modeling the sterilization or inactivation process from a macroscopic viewpoint.

Figure 8 shows the time-dependent temperature profiles at three positions in the sample. The figure also shows the temperature curve measured by the thermocouple (solid line) at the third position.

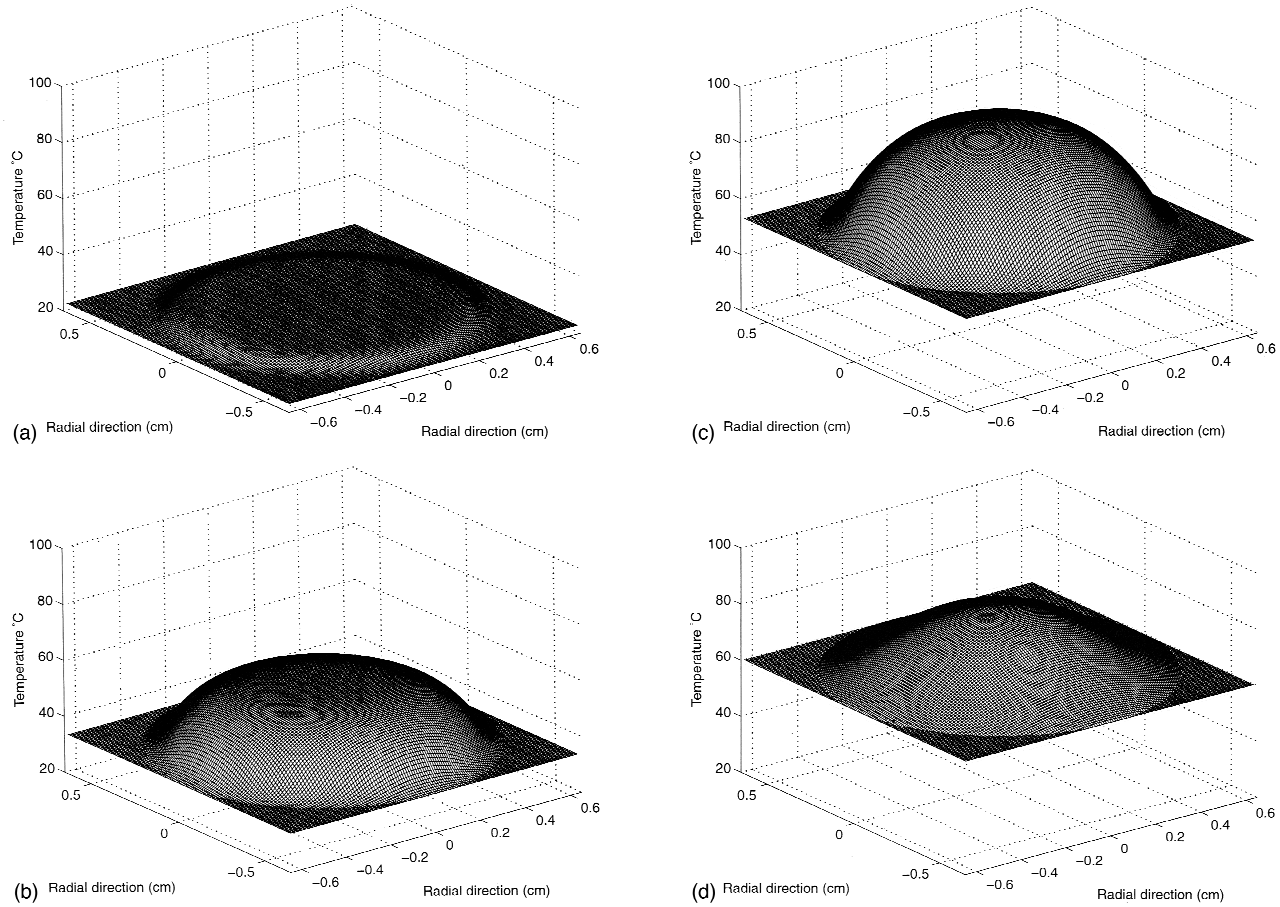

Fig. 5 The transient temperature profiles on the plane that is perpendicular to the central axis and 0.3 cm away from the top surface at the instant of: (a) 1 s, (b) 10 s, (c) 21.6 s, and (d) 35 s, respectively.

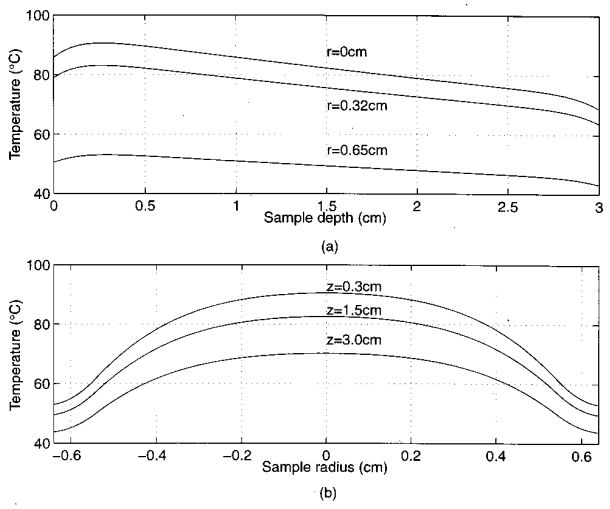

Fig. 6 The temperature profiles (a) as a function of depth for different radial distances from the center of the beam and (b) as a function of radial distance from the center of the beam for different depths.

From Figure 8 it can be seen that the theoretical calculation of the temperature at the positions agreed very well with the temperature obtained from the experimental measurement (the maximum deviation was less than 1.5 °C). This verified the mathematical model. With increasing exposure, the temperature gradient through the vessel became larger and reached its maximum at the time the laser was turned off; it then decreased due to convection and cooling processes. The maximum predicted temperature difference was 45.0 °C.

To further verify the mathematical model, experimental measurement for different conditions were made and compared with the theoretical predictions from the model; the results are illustrated in Fig. 9. In Figure 9(a), the conditions were the same as for Figure 8, but the laser was operated at a pulse repetition rate of 8 Hz and the laser irradiation time was 25.6 s. In Figure 9(b), the conditions were also the same as for Figure 8, but the vessel was changed to one that allowed a suspension depth of 10.5 cm, and three thermocouples were positioned equidistant from the top to bottom. These were

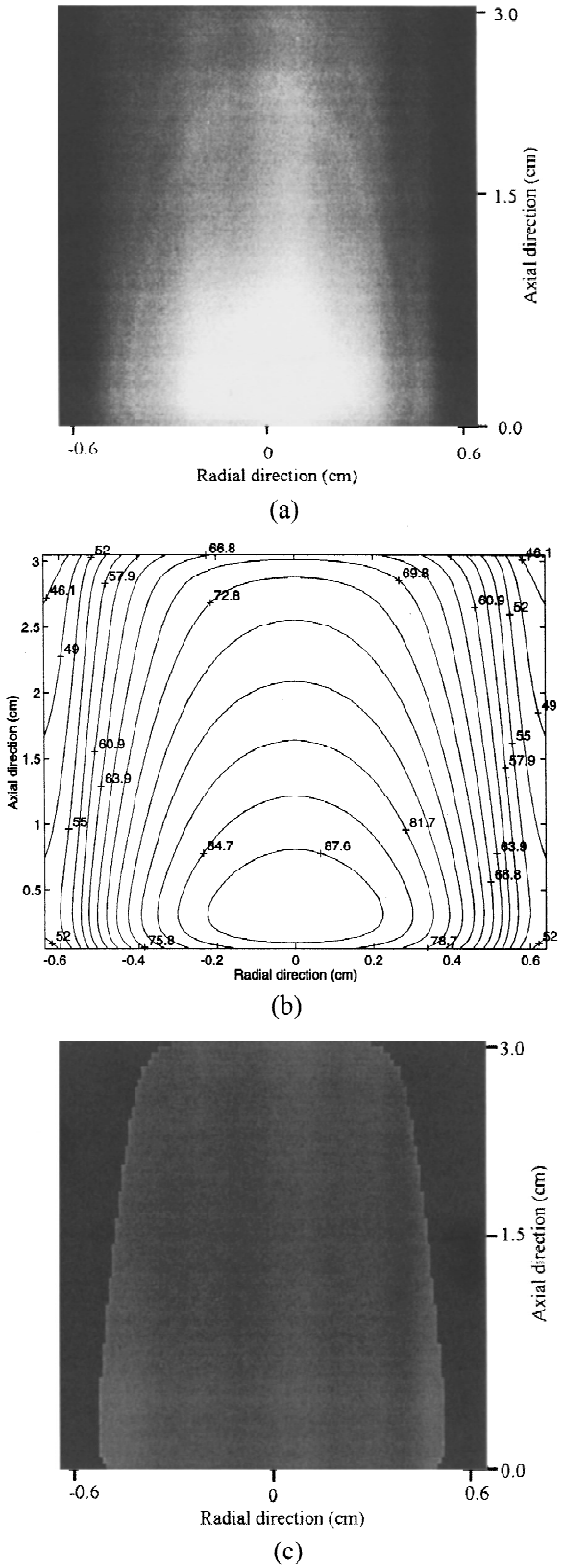

Fig. 7 (a) Gray-level image representation of the temperature profile at the instant the laser was turned off. (b) Contour plot of the isothermal zones of (a). (c) The sterilization zones in a liquid suspension where the gray area represents the sterilized zone and the black region is the area where bacteria could survive.

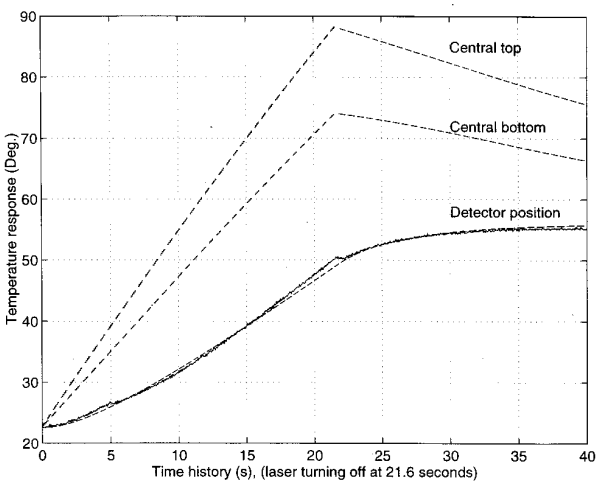

Fig. 8 Time-dependent profiles at three positions in the sample, where the dashed lines were from the theoretical calculation and the solid curve from the experimental measurement. ''Central top'' means the center point at the top surface and ''central bottom'' the center point at the bottom surface.

used to measure the time-dependent temperature profiles at the three different positions. The exposure time was 25.4 s. It can be seen that the results obtained from the theoretical calculations and the experimental measurements are in very good agreement.

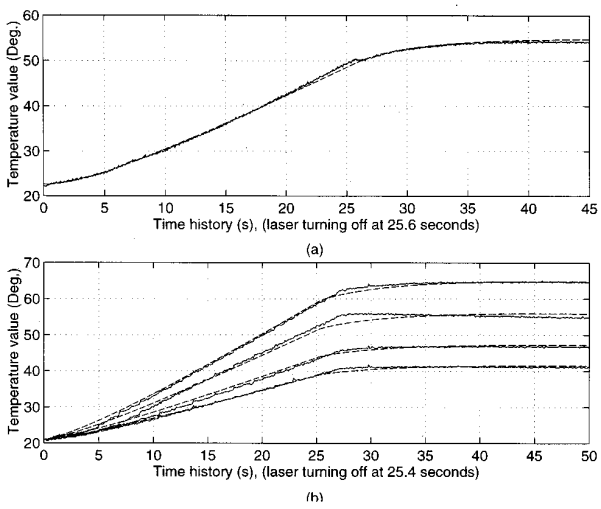

Fig. 9 Theoretical prediction (dashed curve) and experimental measurement (solid line) for different conditions: (a) The conditions were same as for Figure 8 but the laser was operated at a pulse repetition rate of 8 Hz and the laser irradiation time was 25.6 s, (b) The conditions were also same as for Figure 8, but the vessel was changed to one that allowed a suspension depth of 10.5 cm, and three thermocouples were positioned equidistant from the top to the bottom.

5 CONCLUSIONS

A mathematical model was developed to calculate the three-dimensional temperature distribution of a bacterial liquid suspension during laser irradiation. The model has the following advantages:

- The temperature distribution can be calculated under arbitrary combinations of laser wavelength, pulse width, pulse shape, repetition rate, and beam shape, etc.
- Three-dimensional temperature profiles can be obtained at any transient state.
- The model allows the wavelength- and temperature-dependent absorption properties of exposed material to be considered; this makes the prediction of the temperature profile more accurate.
- The model can easily be adapted to be used in other specific applications, such as laser sterilization of solid surfaces or other liquids.

The magnitude of the temperature gradient was quantified in both the radial and axial directions during irradiation. The implication of this work when designing laser sterilization systems is that the laser operating conditions and the thermal and photo properties of the sample are important parameters to be considered. Moreover, the laser beam size, sample size, and the sample depth have to be optimized.

The temperature profiles at particular points in a liquid suspension exposed to laser irradiation under different conditions were experimentally measured. The results were in good agreement with those obtained from the theoretical model. Gray-level images of the treated sample were obtained and these images could be used to predict the level of sterility or inactivation that could be achieved for a given set of operating conditions. We are continuing work to further demonstrate the biological relevance of the model. This will include investigation of the inactivation of bacteria in different zones within the volume of a sample and the extension of the model into a scanning sterilization system, etc.

Acknowledgment

This work was funded by the Ministry of Agriculture, Fisheries and Food, UK, under contract No. FS1033.

REFERENCES

1. N. Saks and C. Roth, ''Ruby laser as a microsurgical instrument,'' *Science*, **141**, 46–47 (1963).
2. G. Powell and B. Whisenant, ''Comparison of three lasers for dental instrument sterilization,'' *Lasers Surg. Med.*, **11**, 69–71 (1991).
3. J. Adrian and A. Gross, ''A new method of sterilization: the CO_2 laser,'' *J. Oral Path.*'' **8**, 60–61 (1979).
4. R. Schultz, F. Cabello, G. Harvey, M. Fernandez-Beros, and S. Krishnamurthy, ''Bactericidal effects of the Nd:YAG laser: *In vitro* study,'' *Lasers Surg. Med.*, **6**, 445–448 (1986).
5. I. A. Watson, G. D. Ward, R. K. Wang, J. H. Sharp, D. M. Budgett, D. E. Stewart-Tull, A. C. Wardlaw, and C. R. Chatwin, ''Comparative bactericidal activities of lasers operating at seven different wavelengths,'' *J. Biomed. Opt.* **1**(4), 466–472 (1996).
6. D. Ward, I. A. Watson, D. E. Stewart-Tull, A. C. Wardlaw, and C. R. Chatwin, ''Inactivation of bacteria and yeasts on agar surfaces with high power Nd:YAG laser-light,'' *Lett. Appl. Microbiol.* **23**, 136–140 (1996).
7. S. L. Jacques, ''Laser-tissue interactions,'' *Surg. Clin. North America*, **72**, 531–558 (1992).
8. S. L. Jacques and S. A. Prahl, ''Modelling optical and thermal distributions in tissue during laser irradiation,'' *Lasers Surg. Med.*, **6**, 494–503 (1987).
9. D. C. Yu, J. L. Fox, J. Hsu, G. L. Powel, and W. I. Higuchi, ''Computer simulation of surface temperature profiles during CO_2 laser irradiation of human enamel,'' *Opt. Eng.* **32**, 298–305 (1993).
10. A. Sagi, A. Shitzer, A. Katzir and S. Akselrod, ''Heating of biological tissue by laser irradiation: theoretical model,'' *Opt. Eng.* **31**, 1417–1424 (1992).
11. J. P. Holman, *Heat Transfer*, 5th ed., McGraw-Hill, Tokyo (1981).
12. K. R. Diller, ''Analysis of skin burns,'' in *Heat Transfer in Medicine and Biology: Analysis and Applications*, A. Shitzer and R. C. Eberhart, Eds., Vol. 2, pp. 85–134, Plenum Press, New York (1985).
13. R. L. Burden, J. D. Faires, and A. C. Reynolds, *Numerical Analysis*, 2nd ed., Prindle, Weber & Schmidt, Boston (1981).
14. A. J. Chapman, *Heat Transfer*, 4th ed., Macmillan, New York (1984).
15. C. B. Allen Yeo, I. A. Watson, R. K. Wang, ''Anomalous optical properties of water at 40 °C and 1.06 μm,'' Cleo/Europe '96, Hamburg, Germany.
16. I. A. Watson, R. K. Wang, G. D. Ward, D. E. S. Stewart-Tull, and A. C. Wardlaw, ''Nd:YAG Laser Sterilization of *E. coli* in liquid,'' to be published.